

## Enhanced thermoelectric properties of lightly Nb doped SrTiO<sub>3</sub> thin films

S. Bhansali<sup>1</sup>, W. Khunsin<sup>1</sup>, A. Chatterjee<sup>1</sup>, J. Santiso<sup>1</sup>, B. Abad<sup>2</sup>, M. Martin-Gonzalez<sup>2</sup>, G. Jakob<sup>3,4</sup>, C. M. Sotomayor Torres<sup>1,5</sup> and E. Chávez-Angel<sup>1\*</sup>

<sup>1</sup> Catalan Institute of Nanoscience and Nanotechnology (ICN2), CSIC and The Barcelona Institute of Science and Technology, Campus UAB, Bellaterra, 08193 Barcelona, Spain

<sup>2</sup> Instituto de Microelectronica de Madrid, IMM-CNM, CSIC, Isaac Newton, 8 PTM, 28760 Tres Cantos (Madrid), Spain

<sup>3</sup> Institut für Physik, Johannes Gutenberg Universität Mainz, Staudingerweg 7, 55128 Mainz, Germany.

<sup>4</sup> Graduate School Materials Science in Mainz, Staudingerweg 9, 55128 Mainz, Germany

<sup>5</sup> ICREA, Passeig Lluís Companys 23, 08010 Barcelona, Spain

\*Corresponding author: e-mail: [emigdio.chavez@icn2.cat](mailto:emigdio.chavez@icn2.cat)

### Target preparation

STO targets doped with 2, 5 and 15 mol% Nb were prepared by a conventional solid-state reaction method. SrCO<sub>3</sub> (Crystec, 99.99% pure), TiO<sub>2</sub> (Crystec, 99.99% pure) and Nb<sub>2</sub>O<sub>5</sub> (Crystec, 99.99% pure) powders were mixed in suitable stoichiometric ratios (2:2:1). The mixture was baked at 1050° C for 48h in a high temperature oven. After that, the powders were ball milled and pressed into bars at 150 MPa and sintered at 1400°C for 48 hours to avoid the formation of the oxygen vacancies.

### X-ray photoelectron spectroscopy (XPS)

XPS data in **Figure S1a** shows the binding energies of the Sr 3d-doublet lines at 133.7 and 135.5 eV which are attributed to Sr 3d<sub>5/2</sub> and Sr 3d<sub>3/2</sub>, respectively. In the case of strontium these values are attributed to  $\alpha$ -Sr.<sup>2</sup> Here, the  $\alpha$ -component corresponds to Sr atoms in the ‘perovskite-like superconductor phase’ of the Nb-SrTiO<sub>3</sub> structure. The binding energies of the Ti 2p<sub>3/2</sub> and Ti 2p<sub>1/2</sub> of Nb-SrTiO<sub>3</sub> samples are 459 and 464.8 eV, and of Nb 3d<sub>5/2</sub> 206.5 eV as shown in (**Figure S1b** and **c**).

These values are close to the reported values for  $\alpha$ -Ti atoms in the perovskite structure of SrTiO<sub>3</sub> and correspond to Ti with oxidation state of 4+ and to no oxidation state of 3+.<sup>2</sup> The absence of peaks around 456 and 462 eV, marked in grey, suggests that oxidation states of Ti<sup>3+</sup> are not present in the films, indicating a non-detectable presence of oxygen vacancies.<sup>2</sup> Finally, the high binding energy shoulder of the O(1s) peak near 532 eV is observed for this surface (**Figure S1d**), consistent with the O(1s) spectra of epitaxial

## Supporting information

SrTiO<sub>3</sub> films hydroxylated due to air exposure<sup>3</sup>. All these measurements were performed on 50 nm thick 2% Nb-doped SrTiO<sub>3</sub> thin film grown on LAO substrate.

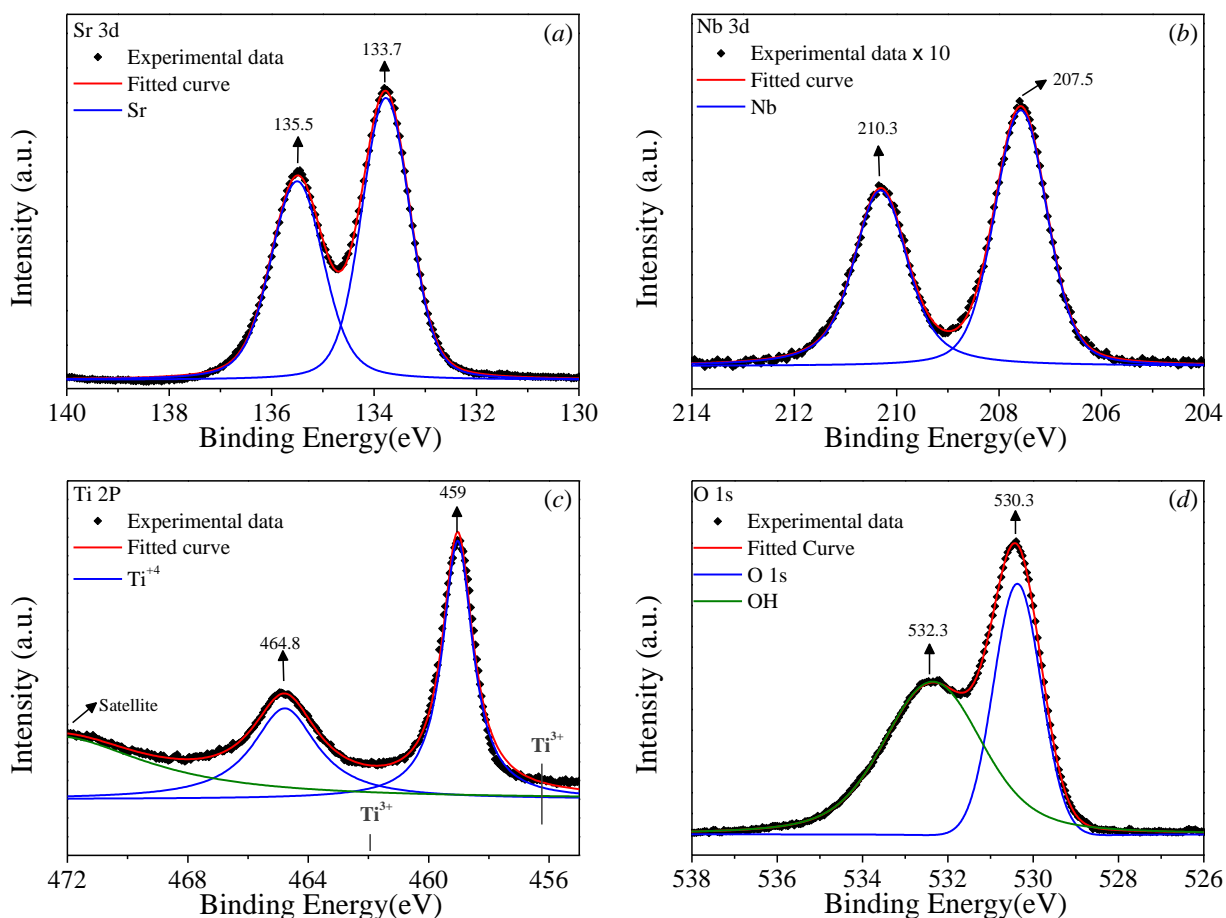


**Figure S1.** XPS spectra of the different elements in the films for 50 nm thick Nb:STO thin film growth in LaAlO<sub>3</sub> substrate.

### High resolution transmission electronic microscopy (HRTEM) and atomic force microscopy (AFM)

**Figure S2a** and **b** shows the high resolution transmission electronic microscopy images of 50, 30 and 200 nm thick 2% Nb-doped SrTiO<sub>3</sub> thin films grown on LAO substrate, respectively. The HRTEM images present evidence of the epitaxial growth and also the variation of the grain boundaries with comparison to the thickness, as can be observed in the insets of each figure. By looking at the AFM surface scans, displayed in **Figure S2c** and **d**, one can notice a remarkable smooth surface of two 50 nm thick 2% Nb-doped SrTiO<sub>3</sub> thin films grown on LAO and lanthanum strontium aluminate (LSAT) substrates. Roughness in the order of 1 nm were detected.

## Supporting information

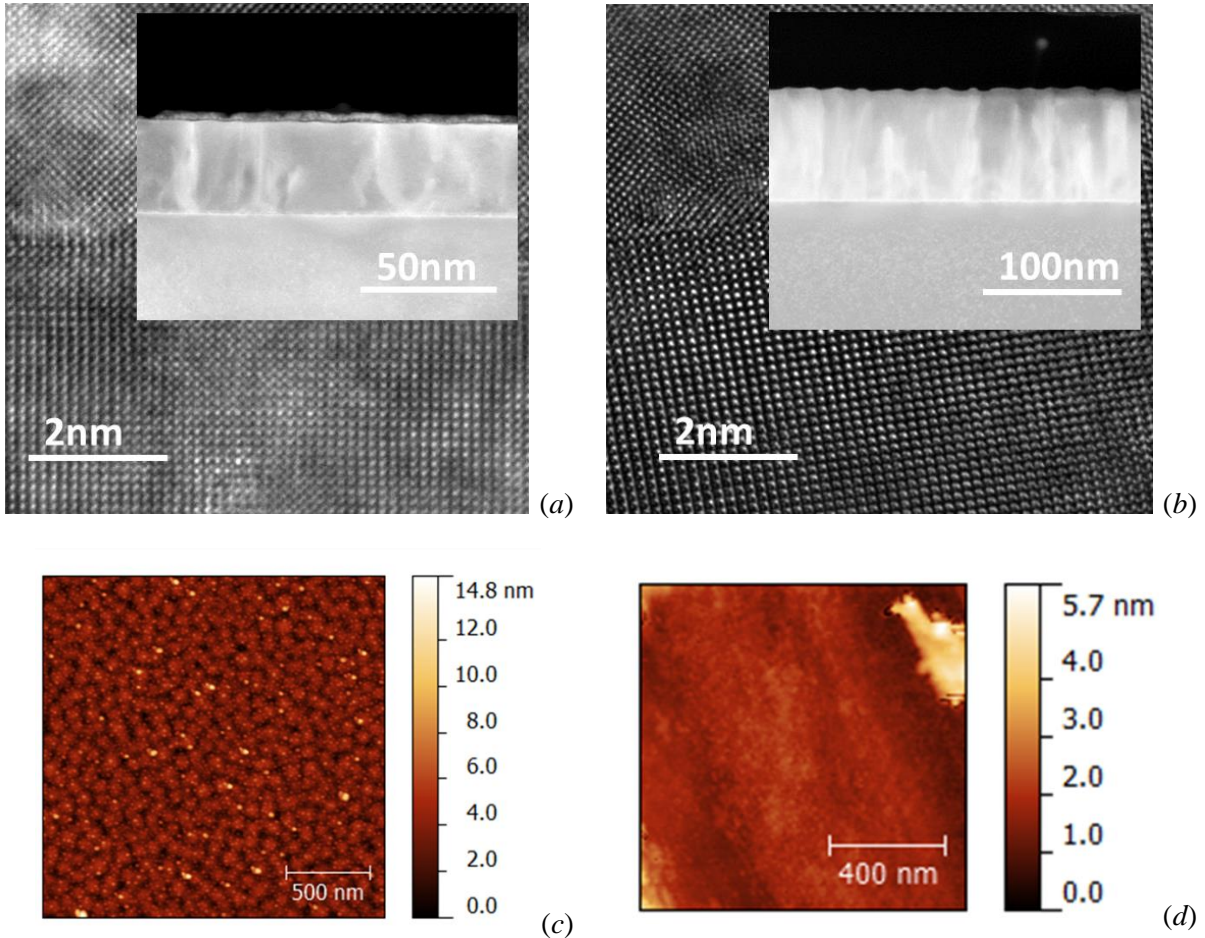


**Figure S2** (a) and (b) HRTEM cross-section image of the interface region showing the substrate and the epitaxial growth of 30 and 200 nm thick thin film of 2% Nb-doped SrTiO<sub>3</sub> grown on LaAlO<sub>3</sub> substrate, respectively. Inlet are the BF-STEM images showing the variation of the grain boundaries in the 30 and 200 nm thick film, respectively. (c) and (d) AFM images of Nb:STO on LaAlO<sub>3</sub> and (b) lanthanum strontium aluminate (LSAT) substrates showing roughness < 1nm.

### X-ray diffraction analysis

In the x-ray diffraction (XRD) patterns of as-sintered target samples shown in **Figure S3a**, some unexpected weak peaks are found around  $2\theta = 28^\circ$ , implying the presence of a second rutile phase (TiO<sub>2</sub> or Nb-doped TiO<sub>2</sub>). According to the defect chemistry model, the donor compensation mechanism should shift from the cation vacancy to the electronic type.<sup>1</sup> It is also noted that the lattice constant estimated from Rietveld refinement (red dashed line) increases with increasing doping level. Such increase in the cell volume is related to the replacement of small-sized Ti<sup>4+</sup> ions (60.5 pm) in the B site of the perovskite structure by the larger Nb<sup>5+</sup> ions (64.0 pm). This donor compensation mechanism also supports the increase of the unit-cell volume upon replacement of Ti<sup>4+</sup> ions by Nb<sup>5+</sup> ions.

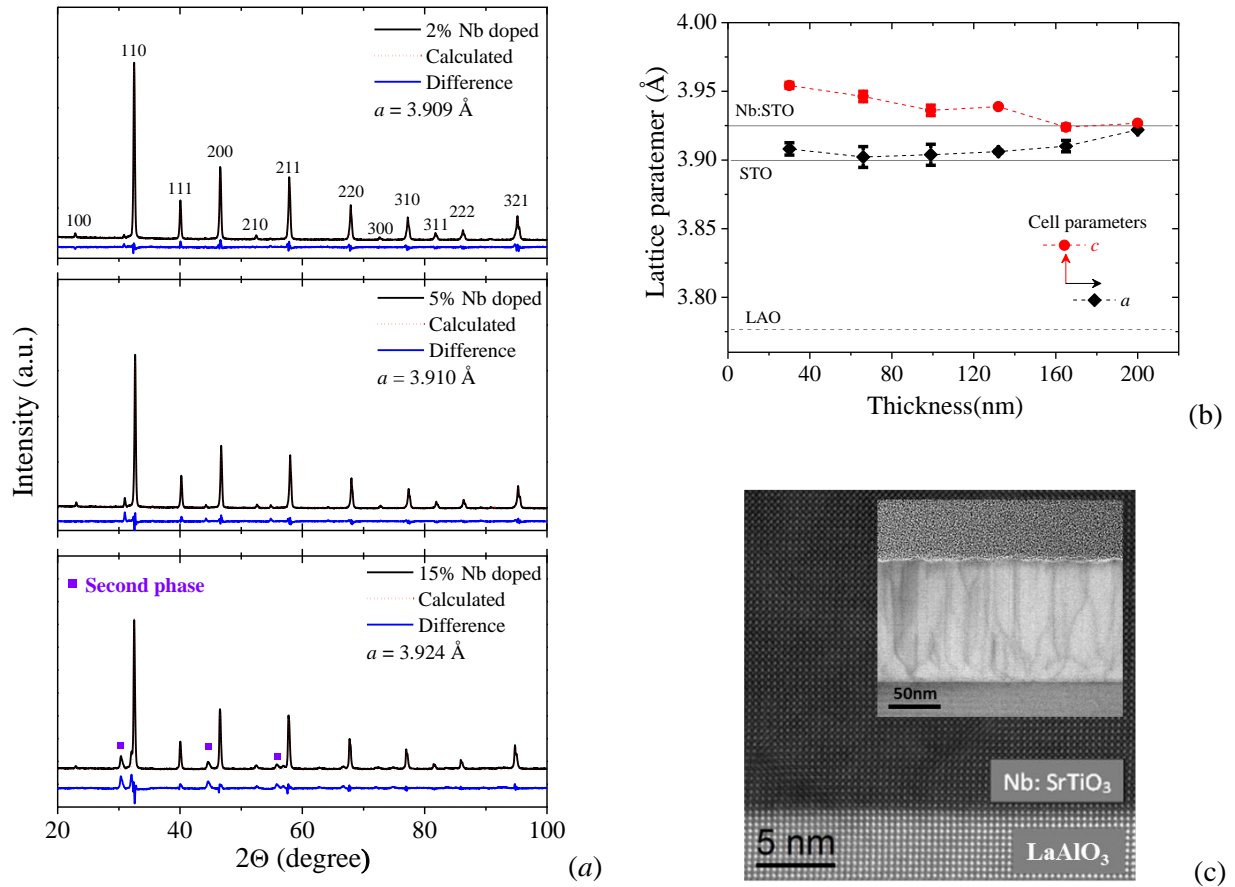


**Figure S3** (a) XRD pattern of 2, 5 and 15% mol Nb-doped SrTiO<sub>3</sub> targets (b) In-plane and out-of-plane lattice parameters calculated from reciprocal space maps as function of film thickness for 2% Nb-doped STO samples grown on LaAlO<sub>3</sub> substrates. (c) HRTEM cross-section image of the interface region showing the substrate and the epitaxial growth of the 50 nm thick thin film of Nb-doped SrTiO<sub>3</sub> on LaAlO<sub>3</sub> substrate and inset is the BF-STEM image showing the variation of the grain boundaries in the film.

**Figure S3b** shows the in-plane ( $a$ -constant) and out-of-plane ( $c$ -constant) lattice parameters of 2% Nb-doped SrTiO<sub>3</sub> films as function of film thickness grown on LaAlO<sub>3</sub> (LAO) substrate. The lattice constants were estimated from reciprocal space maps of each sample (not shown here).

### Seebeck and power factor of 2% Nb-doped on LAO

**Figure S4** shows the temperature dependence of the Seebeck coefficient and the power factor for the different Nb-doped STO thin films deposited on LAO substrates. The experimental measurements did not show a large temperature dependence of both quantities.

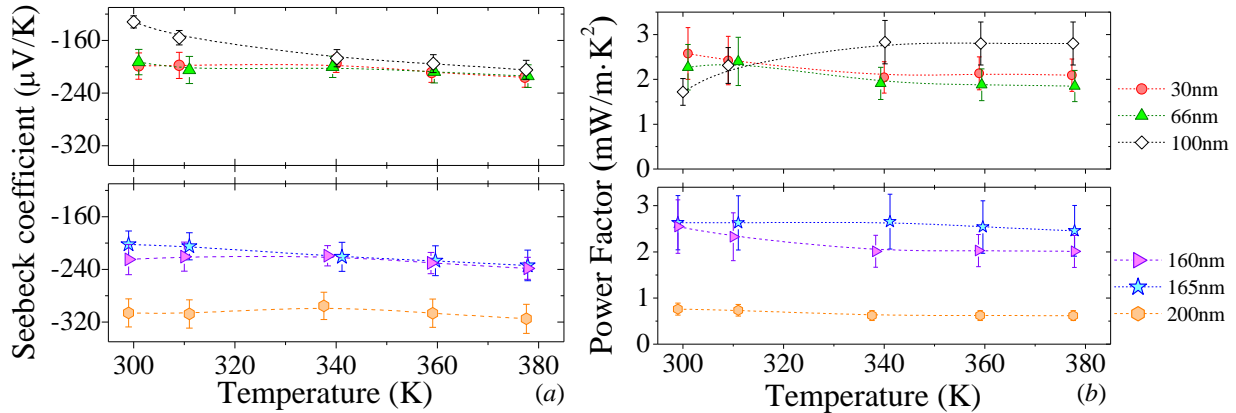


**Figure S4** Temperature dependence of the (a) Seebeck coefficient and (b) power factor for six different 2% Nb-doped thin films grown on LAO substrates.

### Thermal conductivity

To measure the thermal conductivity ( $k$ ) of our grown thin film, we have employed our home-built three-omega ( $3\omega$ ) method<sup>4</sup>. In comparison to other methods of measuring  $k$ , the  $3\omega$  technique, via its use of the frequency dependence of temperature oscillations, offers several major advantages including eliminating errors from black-body radiation and reducing thermalisation time.<sup>5,6</sup> The principle of operation is based on the use of a thin electrically conductive wire deposited on the specimen to be measured, which acts as a heater and thermometer at the same time. The wire was fabricated by depositing 50 nm thick of gold using DC-sputtering directly on the sample. Later, the  $3\omega$ -heater is patterned by photolithography and etching of gold thin film, grown in situ just after the deposition of 200 nm thick  $\text{AlO}_x$  electrical insulation layer. An extended description of the method and the associated error in the measurement can be found in the supporting information of the reference [7]. **Figure S5a** shows the electrical resistance of the  $3\omega$ -wire as function of temperature of 10 and 60 nm thick 2% Nb-doped  $\text{SrTiO}_3$  thin films grown on  $\text{MgO}$  substrates. The thinnest sample acts as references while the thicker one will be the sample under study. To extract the thermal conductivity of the film under study, we can model the film as a frequency independent thermal resistance where the heat will flow from heater to the substrate. In this case the Fourier law can be applied in one dimension as follows:

## Supporting information

$$\begin{aligned}
 P = Q &= kA_{int} \frac{\Delta T_f}{d_f} \approx 2klb \frac{\Delta T_f}{d_f} \\
 \rightarrow k &= \frac{Pd_f}{2lb\Delta T_f}
 \end{aligned}
 \tag{1}$$

where  $P$  is the input power applied to the  $3\omega$ -heater,  $Q$  is the modulus of the heat flow,  $A_{int}$  is the area below the heater strip ( $A_{int} = 2lb$ , where  $l$  is heater length and  $b$  is half width of heater),  $\Delta T_f$  is the temperature rise of the film and  $d_f$  is the film thickness. Since the  $3\omega$  measurement gives only the temperature rise between top (heater-sample) and bottom of the whole sample (interface of sample to the infinite sink), it is not possible to measure  $\Delta T_f$  directly. However, if a sample is created that not only consists of the film of interest, but also adds a small reference, the measurable system temperature increase ( $\Delta T_{sys}$ ) can be superimposed by the  $\Delta T_f$  and the  $\Delta T_r$  of the system containing the substrate and the reference (see **Figure S5b**). Then the temperature rise of the system can be expressed as:

$$\Delta T_{sys} = \Delta T_r + \Delta T_f \tag{2}$$

The  $\Delta T_r$  is obtained directly by measuring other sample that contains only the substrate and the reference film. Finally, the thermal conductivity of the film of interest is obtained by subtracting the  $\Delta T_{sys}$  and  $\Delta T_f$  and given by:

$$k = \frac{Pd_f}{2bl(\Delta T_{sys} - \Delta T_r)} \tag{3}$$

where  $d_f$  is the thickness of the film after the subtraction of the reference sample, i.e.,  $d_f = 60 \text{ nm (sample + reference)} - 10 \text{ nm (reference)} = 50 \text{ nm}$ .

The thermal conductivity of MgO substrate was obtained from the slope of both temperature rise as it shown in grey ( $k_{sub} = 51.82 \text{ W m}^{-1} \text{ K}^{-1}$ ) and orange ( $k_{sub} = 52.41 \text{ W m}^{-1} \text{ K}^{-1}$ ) for the reference and the film under study, respectively. The bulk thermal conductivity measured here are in very good agreement to the widely accepted at room temperature  $k_{MgO} = 50 \text{ W m}^{-1} \text{ K}^{-1}$ .<sup>8,9</sup> Finally, the thermal conductivity of the sample under study was estimated to be  $k_{film} = 5.44 \pm 1.0 \text{ W K}^{-1} \text{ m}^{-1}$ .

## Supporting information

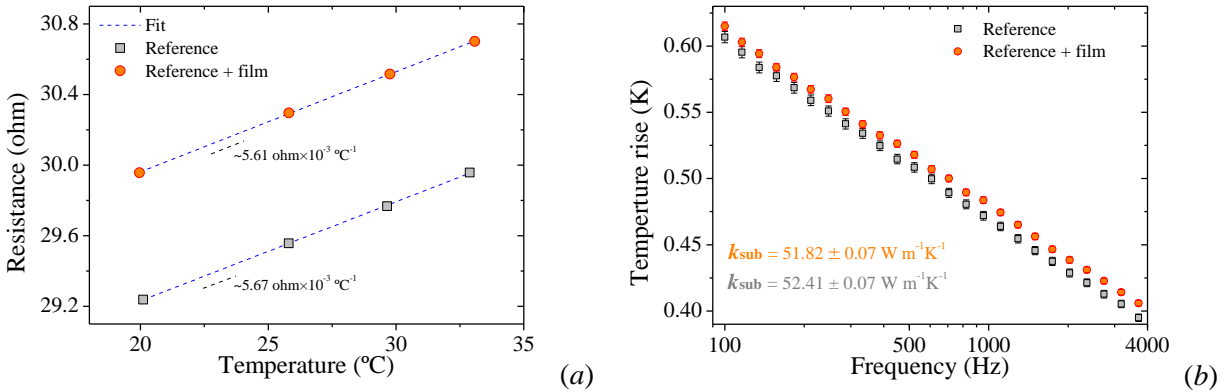


**Figure S5** (a) electrical resistance as a function of temperature of  $3\omega$ -strip deposited on reference (grey squares) and reference plus film samples (orange circles). (b) Temperature rise of the reference (grey squares) and the sample under study (orange circles) as function of excitation frequency. From the slope of each measurement the thermal conductivity of the substrate was also determined as is shown in grey and orange, respectively.

## References

- 1 T. Kolodiazhnyi and A. Petric, *J. Electroceramics*, 2005, **15**, 5–11.
- 2 M. S. J. Marshall, D. T. Newell, D. J. Payne, R. G. Egdell and M. R. Castell, *Phys. Rev. B*, 2011, **83**, 35410.
- 3 S. A. Chambers, Y. Liang, Z. Yu, R. Droopad and J. Ramdani, *J. Vac. Sci. Technol. A Vacuum, Surfaces, Film.*, 2001, **19**, 934–939.
- 4 P. Hołuj, C. Euler, B. Balke, U. Kolb, G. Fiedler, M. M. Müller, T. Jaeger, E. Chávez Angel, P. Kratzer and G. Jakob, *Phys. Rev. B*, 2015, **92**, 125436.
- 5 D. G. Cahill, *Rev. Sci. Instrum.*, 1990, **61**, 802.
- 6 D. G. Cahill, *Rev. Sci. Instrum.*, 2002, **73**, 3701.
- 7 E. Chavez-Angel, N. Reuter, P. Komar, S. Heinz, U. Kolb, H.-J. Kleebe and G. Jakob, *Nanoscale Microscale Thermophys. Eng.*, 2019, **23**, 1–9.
- 8 D. G. Cahill, Thermal conductivity bulk single crystal MgO; Temperature dependence of volumetric heat capacity MgO. Department of Materials Science and Engineering. University of Illinois at Urbana Campaign, <http://users.mrl.illinois.edu/cahill/tcdata/tcdata.html>, (accessed 1 January 2016).

## Supporting information

- 9 E. Langenberg, E. Ferreiro-Vila, V. Leborán, A. O. Fumega, V. Pardo and F. Rivadulla, *APL Mater.*, 2016, **4**, 104815.